Properties of high temperature superconductors in states of mixed symmetry

2008 J. Phys.: Condens. Matter 20 255218

(http://iopscience.iop.org/0953-8984/20/25/255218)

J. Phys.: Condens. Matter **20** (2008) 255218 (12pp) doi:10.1088/0953-8984/20/25/255218

Properties of high temperature superconductors in states of mixed symmetry

Madhuparna Karmakar and Bishwajyoti Dey

Department of Physics, University of Pune, Pune 411007, India

E-mail: madhu@physics.unipune.ernet.in and bdey@physics.unipune.ernet.in

Received 29 October 2007, in final form 26 April 2008
Published 21 May 2008
Online at stacks.iop.org/JPhysCM/20/255218

Abstract

We study the properties of high temperature superconductors (HTSs) in the states of mixed symmetry with coexisting d- and s-wave order parameter components. We model the mixed symmetry states of the HTSs in the framework of two-order-parameter Ginzburg–Landau (GL) theory. We solve the coupled nonlinear GL equations using a high precision exact numerical iteration technique for the entire range of applied magnetic field, arbitrary GL parameter κ and vortex lattice symmetry. We study theoretically and compare with experiments several properties of HTSs, such as local spatial behaviors of the magnetic field and order parameter profiles, vortex core radius, penetration depth of the magnetic field, structure of the vortex lattice, reversible magnetization, upper critical field H_{c2} and shear modulus of the vortex lattice, and their variations with temperature and applied magnetic field. The excellent agreement between theoretical and experimental results on HTSs shows that the mixed symmetry scenario is a good candidate for the description of the HTSs.

1. Introduction

A major topic of interest and discussion in high-T_c cuprate superconductors is the pairing symmetry of the superconducting order parameter, which appears to be a crucial step in the identification of the pairing mechanism and in the subsequent development of a microscopic theory for the high-T_c superconductors. There is growing evidence that the symmetry of the order parameter in high-T_c cuprate superconductors is different from the low-T_c superconductors, most of which have s-wave pairing symmetry. For high-T_c cuprate superconductors there is strong experimental evidence that the spin pairing is singlet [1], thereby suggesting an s-wave or d-wave pairing state. But in strongly correlated electron systems, the s channel can be blocked by the strong on-site Coulomb repulsion, leaving open the possibility of a higher-angular-momentum d-wave pairing state. Several experiments have been interpreted for the possibility of a d-wave symmetry, i.e. the $d_{x^2-y^2}$ pairing state with lines of nodes in the energy gap. Experiments which directly probe the pairing symmetry by using phase sensitive devices such as Josephson junctions and superconducting quantum interference devices (SQUIDs) have supported the possibility of a d-wave pairing symmetry [2–5]. Similarly, the observed polarization dependence of the Raman scattering experiments has been accounted for by a $d_{x^2-y^2}$ pairing state [6]. However, many of the inconsistencies in these experimental results can be interpreted by allowing for states of a mixture of s- and d-wave symmetric order parameters. The origin of the mixed phase consisting of both s and d components has been explained as due to the introduction of a small orthorhombic distortion in the CuO_2 plane resulting from the existence of the CuO chains [7]. The mixing of the s- and d-waves due to the orthorhombic distortion results in the anisotropy of the gap between the x and y directions [8]. Such anisotropy has been observed in the Raman scattering experiments of $YBa_2Cu_4O_8$ [9] and $YBa_2Cu_3O_7$ [10] and more recently in the photo-emission spectra from $YBa_2Cu_3O_{7-\delta}$ [11]. Similarly, there are several experiments, which, even though they are consistent with predominantly $d_{x^2-y^2}$ pairing symmetry, do not rule out a mixture of s-wave component, like the field modulated critical current measurement experiment to obtain the pairing state symmetry of $YBa_2Cu_3O_{7-\delta}$ [12], momentum resolved temperature dependence of the superconducting gap of $Bi_2Sr_2CaCu_2O_{8+x}$ [13], observation of Josephson supercurrents along the c direction in YBCO–Pb superconductor–insulator–superconductor tunnel junctions [14], thermal

conductivity measurements of $YBa_2Cu_3O_{7-\delta}$ detwinned single crystal [15] etc. Most recent angle-resolved electron tunneling experiments of Smilde *et al* [16] also show the formation of states of mixed symmetry, where the major bulk pairing mechanism is d wave in nature with a sub-dominant admixture of s-wave pairing. For other experiments which are compatible with the mixed symmetry states of d and s waves with the former being the dominant component, we refer to the review article [17].

The mixed symmetry scenario has been suggested as the origin of many experimentally observed unusual effects in HTSs, such as the unusual upward curvature of the plot of thermodynamic H_{c2} versus temperature [18], the pseudo-gap effects in HTSs [19], nonmagnetic impurity effects in HTSs leading to an energy gap [20] and superconducting fluctuation effects in HTS [21]. Recent small angle neutron scattering (SANS) and scanning tunneling microscopy experiments on high T_c superconductors YBCO [22] have shown anomalous magnetic field dependence of the vortex lattice structure. It has been proposed that this effect can arise from including two or more order parameters (such as s and d) in the Ginzburg–Landau (GL) free energy, with derivative mixing terms reflecting the ionic lattice symmetry [23]. Similarly, a two-component order parameter theory has been used to describe the observed anomalous properties of the heavy fermion superconductor UPt_3 [24]. In the case of heavy fermion metal UPt_3, measurements of the low temperature ultrasonic attenuation, specific heat, nuclear spin relaxation and thermal conductivity all show qualitatively different behavior from that predicted by the BCS theory for a conventional superconductor (for review see Fisk *et al* [25]).

The study of the single vortex and vortex lattice structure of a superconductor is very important for determining the transport property and pairing symmetry of the order parameter. Studying the symmetry properties of the core of d-wave superconductors, Volovik [26] concluded the existence of mixed d- and s-wave pairing in high-T_c superconductors. Ren *et al* [27] derived microscopically the GL equations of HTSs with d-wave symmetry and studied the structure of the single vortex by solving the corresponding GL equations. Similarly, Soininen *et al* [28] calculated the vortex structure numerically within the framework of the self-consistent Bogoliubov–de Gennes theory and identified a region where d- and s-waves coexist. Xu *et al* [29], Heeb *et al* [30], Franz *et al* [31], Ichioka *et al* [32] and Mel'nikov *et al* [33] studied numerically the structure of the single vortex and vortex lattice employing a two-component (s- and d-wave) GL theory and found that an s-wave component of the order parameter is always induced with a fourfold structure and the vortex lattice has oblique structure. Similar numerical studies by Li *et al* showed that the structure of the single vortex in the $d + is$ state exhibits twofold symmetry [34].

One of the major limitations of the above mentioned studies of single vortex and vortex lattice structure in the framework of GL theory is that these are restricted to the applied magnetic fields near the upper and lower critical fields, $H \approx H_{c2}$ and $H \to H_{c1}$, for the vortex lattice and isolated vortices, respectively. These studies are basically limited to solving approximately the coupled two-order-parameter (s- and d-wave) nonlinear GL equations by linearizing the equations [31]. However, experimental studies of small angle neutron scattering (SANS) and scanning tunneling microscopy on high T_c superconductor YBCO have shown the intermediate magnetic field region $H_{c1} \ll H \ll H_{c2}$ to be the most relevant as it has anomalous magnetic field dependence of the vortex lattice structure [22, 35]. In the intermediate field region $H_{c1} \ll H \ll H_{c2}$, the nonlinear GL equations cannot be linearized and it is very difficult to solve the coupled two-order-parameter nonlinear GL equations. Yet another limitation of these studies of isolated vortex and vortex lattice structure of high T_c superconductors in mixed symmetry state is the use of an ansatz for the form of the s-wave symmetry order parameter, thereby reducing the coupled two-order-parameter problem to an approximate effective single-order-parameter model [23, 33].

In this paper we study theoretically the properties of high temperature superconductors in states of mixed symmetry. In particular we are interested in studying the effects of the presence of an additional s-wave order parameter and its coupling with the d-wave order parameter on the vortex states of the HTS. We study in detail the local spatial behavior, the width and peak amplitude of the order parameters and the magnetic field induction, the structure of the single vortex and the vortex lattice and their variations with the parameter representing the gradient coupling between the order parameters. The changes in these local spatial behaviors have a direct reflection on the experimentally observable characteristic properties of the superconductors, such as the vortex core radius, penetration depth of the magnetic field, upper critical applied field H_{c2}, reversible magnetization and the shear modulus of the vortex lattice. We model the HTS in states of mixed symmetry in the framework of two-order-parameter GL theory. Since we are interested in studying the properties of the high T_c superconductors in the entire range of the applied field, we do not linearize the coupled nonlinear GL equations. We also do not use any ansatz for the form of the s-wave order parameter components. Thus, we solve the fully nonlinear coupled two-order-parameter GL equations for the entire range of the applied magnetic field for arbitrary values of the GL parameter (κ) and vortex lattice symmetry. We have studied the effect of the additional order parameter on single vortex and vortex lattice structure, width and amplitude of the order parameters and magnetic induction and their variations with applied magnetic field and the coupling parameter representing the strength of the gradient coupling between the order parameters. We present, for the first time, theoretical calculations and comparison with experiments on various properties of HTSs in states of mixed symmetry, such as coherence length and penetration depth, reversible magnetization, upper critical magnetic field H_{c2}, shear modulus of the vortex lattice and their variations with temperature and applied magnetic field. These properties are a signature of the superconducting phase. The agreement between the theoretical and experimental results is shown to be excellent.

The paper is organized as follows. Section 2 describes the theoretical formalism. In section 3 we give the details of

the analytical and numerical calculations of various properties of HTSs in states of mixed symmetry, discussions and comparison of the analytical results with available experiments on high-T_c superconducting materials. Finally, in section 4 we conclude with suggestions for future work.

2. Theoretical formalism

The two-dimensional average GL free energy density of the high T_c superconductors involving mixed symmetry states can be expressed in terms of the two order parameters of s($\mathbf{r}$)-wave and d($\mathbf{r}$)-wave symmetry as [23, 31]

$$\begin{aligned} f = \langle\, & \alpha_s|s|^2 + \alpha_d|d|^2 + \beta_1|s|^4 + \beta_2|d|^4 \\ & + \beta_3|s|^2|d|^2 + \beta_4(s^{*2}d^2 + d^{*2}s^2) + \gamma_s|\mathbf{\Pi}s|^2 \\ & + \gamma_d|\mathbf{\Pi}d|^2 + \gamma_v[(\Pi_y s)^*(\Pi_y d) - (\Pi_x s)^*(\Pi_x d) \\ & + \text{c.c}] + B^2/8\pi \rangle \end{aligned} \tag{1}$$

where $\mathbf{\Pi} = -i\nabla - \frac{e^*\mathbf{A}}{\hbar c}$, $\alpha_s = \alpha(T - T_s)$, $\alpha_d = \alpha(T - T_d)$ with $(T_s < T_d)$ and $\langle \cdots \rangle = \frac{1}{V}\int d\mathbf{r} \cdots$ denotes the spatial average. Here, we take the two-dimensional spatial average of the free energy to obtain the free energy density. The GL equations are obtained by minimizing the free energy density. $\mathbf{B} = B\hat{z} = \nabla \times \mathbf{A}$ is the local field. H and $\bar{B} = \langle B(x, y)\rangle$ are along z. β_1, β_2, β_3, β_4, γ_s, γ_d and γ_v are all positive quantities. The parameters γ are related to the effective mass, with $\gamma_i = \hbar^2/2m_i^*$, for $i = s, d, v$.

The choice of the parameters considered in our study is determined by the condition of stability of the pure d-wave state in the bulk in the absence of perturbations, i.e. when $|d| > 0$, $s = 0$. The condition for such a state to be thermodynamically stable is given by [28, 31]

$$\alpha_d < 0, \qquad 2\beta_2\alpha_s + (\beta_3 - 2|\beta_4|)|\alpha_d| > 0. \tag{2}$$

In the absence of the parameter ϵ_v the pure d-wave state is stable against admixture of s-wave through the β_3 and β_4 terms (as shown from linear stability analysis [30]). Thus, the β_3 and β_4 terms are not relevant to generate the s-wave component. Therefore, the mixed gradient term, which is proportional to the parameter ϵ_v, is crucial for our problem, and this term gives the maximum contribution to the effects of s-wave mixing. For example, the experimentally observed oblique vortex lattice is reproduced analytically from our calculations only for nonzero values of the parameter ϵ_v, while for $\epsilon_v = 0$ the triangular vortex lattice is realized as in the case of the pure d-wave solution.

We write the order parameters as $s = \sqrt{\omega_s}\exp[i\phi_s]$, $d = \sqrt{\omega_d}\exp[i\phi_d]$ with $\omega_s = |s|^2 \leqslant 1$, $\omega_d = |d|^2 \leqslant 1$ and introduce a gauge invariant real quantity $\mathbf{Q}(x, y) = \mathbf{A}(x, y) - \nabla\phi(x, y)/\kappa$. The supervelocity $-\mathbf{Q}(x, y)$ denotes the gauge invariant velocity of the superconducting electrons. It is related to the current density as $\mathbf{j} = -\mathbf{Q}\omega$, where $\omega(x, y)$ is the density of the superconducting electrons. The word 'supervelocity' was coined by Abrikosov [36] because of the similarity between the spatial variations of the magnitude of $\mathbf{Q}$ (i.e. $Q \to 0$ for $r \to \infty$ and $Q \to 1/\kappa r$ for $r \to 0$) and the superfluid velocity $\mathbf{v}_s$ in helium II. The corresponding three GL equations obtained by minimizing the free energy density, using the variational technique $\delta f/\delta\omega_i = 0$ $(i = s, d)$ and $\delta f/\delta\mathbf{Q} = 0$, can be written as

$$\begin{aligned} \nabla^2\omega_s + 2\kappa^2[& -\alpha_s\omega_s - 2\beta_1{\omega_s}^2 - (\beta_3 + 2\beta_4\cos(2\phi))\omega_s\omega_d \\ & - g_s - \omega_s Q^2 - \epsilon_v\{\cos(\phi)(Q_y^2 - Q_x^2)(\omega_s\omega_d)^{1/2} \\ & + (\omega_s/\omega_d)^{1/2}[\cos(\phi)\{(\nabla_x^2 - \nabla_y^2)\omega_d/2\kappa^2 + g_{dy} - g_{dx}\} \\ & + 2\sin(\phi)(Q_x\nabla_x - Q_y\nabla_y)\omega_d/2\kappa]\}] = 0 \end{aligned} \tag{3}$$

$$\begin{aligned} \nabla^2\omega_d + 2\kappa^2[& \omega_d - 2\beta_2{\omega_d}^2 - (\beta_3 + 2\beta_4\cos(2\phi))\omega_s\omega_d \\ & - g_d - \omega_d Q^2 - \epsilon_v\{\cos(\phi)(Q_y^2 - Q_x^2)(\omega_s\omega_d)^{1/2} \\ & + (\omega_d/\omega_s)^{1/2}[\cos(\phi)\{(\nabla_x^2 - \nabla_y^2)\omega_s/2\kappa^2 + g_{sy} - g_{sx}\} \\ & + 2\sin(\phi)(Q_y\nabla_y - Q_x\nabla_x)\omega_s/2\kappa]\}] = 0 \end{aligned} \tag{4}$$

$$\begin{aligned} \nabla^2\mathbf{Q} - (\omega_s + \omega_d)\mathbf{Q} - \epsilon_v[& 2\cos(\phi)(\omega_s\omega_d)^{1/2}(\hat{\mathbf{y}}Q_y - \hat{\mathbf{x}}Q_x) \\ & + \sin(\phi)\{(\omega_d/4\kappa^2\omega_s)^{1/2}(\nabla_y - \nabla_x)\omega_s \\ & - (\omega_s/4\kappa^2\omega_d)^{1/2}(\nabla_y - \nabla_x)\omega_d\}] = 0 \end{aligned} \tag{5}$$

where $\epsilon_v = \gamma_v/\gamma_d$, $\phi = \phi_d - \phi_s$ is the phase difference and $g_i = (\nabla\omega_i)^2/4\kappa^2\omega_i$, $g_{ij} = (\nabla_j\omega_i)^2/4\kappa^2\omega_i$ for $i = s, d$, $j = x, y$.

We solve the fully nonlinear two-order-parameter GL equations for the entire range of the applied field and for arbitrary values of the GL parameter κ and vortex lattice symmetry using a high precision numerical iterative method [37]. The method basically consist of expressing the order parameters and the magnetic induction as Fourier series. The Fourier coefficients are then determined numerically by iterating the three iterative equations for the Fourier coefficients obtained from the three nonlinear GL equations for the two order parameters and the magnetic induction. Two additional iterative equations for the Fourier coefficients are set up to make the iteration process faster and more stable. These additional two equations are obtained from the minimization conditions of the free energy w.r.t. the amplitudes of the order parameters. This iterative method produces numerically exact solutions of the fully nonlinear GL equations valid for the entire range of the applied magnetic field $H_{c1} < H < H_{c2}$ for arbitrary value of Ginzburg–Landau parameter and vortex lattice symmetry [37].

3. Numerical calculations, results and discussions

The solutions of the coupled nonlinear GL equations involving two order parameters and the magnetic field are computed numerically using the iterative method as discussed above. We compute various properties of HTSs and their variations with temperature and the applied magnetic field (parameter $b = \bar{B}/B_{c2}$). In particular, we compute the variations with the coupling parameter ϵ_v, which represents the gradient coupling between the order parameters, to examine the effects of the existence of an additional order parameter on the properties of the system.

3.1. Single vortex and vortex lattice structure

We denote the vortex positions in the vortex lattice as $\mathbf{R} = \mathbf{R}_{mn} = (mx_1 + nx_2, ny_2)$ (m, n integer). For the triangular lattice, one has $x_2 = x_1/2$, $y_2 = x_1\sqrt{3}/2$, and for the square lattice $x_2 = 0$, $y_2 = x_1$. We first determine the structure

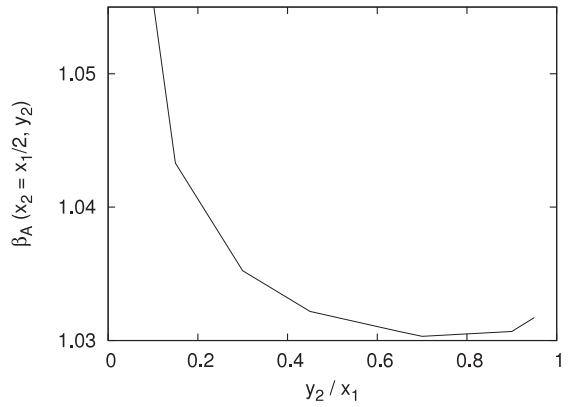

Figure 1. Variation of Abrikosov parameter β_A with lattice symmetry parameter y_2. Parameter values used are $\alpha_s/|\alpha_d| = 0.5$, $\beta_1/2\beta_2 = \beta_3/2\beta_2 = 1.0$, $\beta_4/2\beta_2 = 0.5$, $\epsilon_v = 0.4$, phase difference $\phi = (\phi_d - \phi_s) = \pi/2$, $\kappa = 72$ and magnetic induction $b = 0.8$.

of the vortex lattice of HTSs in states of mixed symmetry. This can be done by determining the dependence of the free energy $f(x_2 = x_1/2, y_2)$ on y_2 and finding the value of y_2 which minimizes the free energy. An easier alternative approach to obtain the same information is to find the value of y_2 which minimizes the Abrikosov parameter (see [31]). The Abrikosov parameter is defined as $\beta_A = \langle\omega_s^2\rangle/\langle\omega_s\rangle^2$. Figure 1 shows the variation of the Abrikosov parameter with y_2 for a particular value the coupling parameter ϵ_v ($\epsilon_v = \gamma_v/\gamma_d$), the coefficient of mixed gradient coupling terms. We have taken the value of the GL parameter $\kappa = 72$ which is obtained from the experiments on YBCO [35]. For $\epsilon_v = 0.4$, β_A is minimum for $y_2 = 0.71$ (we take $x_1 = 1$). The vortex lattice is thus oblique. This is in agreement with the experimentally observed oblique vortex lattice structure of YBCO [22].

Changing the value of the coupling parameter ϵ_v results in a change in the value of y_2 for which β_A is minimum. For $\epsilon_v = 0.1, 0.2, 0.3, 0.4$ and 0.5, β_A is minimum at $y_2 = 0.44, 0.48, 0.55, 0.71$ and 0.74, respectively. The overall structure of the vortex lattice remains oblique.

Figure 2 shows the contour plots for the order parameter components $\omega_s(x, y)$ and $\omega_d(x, y)$ for three different values of the coupling parameter ϵ_v. It can be seen that the variation in the value of parameter ϵ_v results in variation in the structure of the vortex lattice, though the lattice remains in general oblique.

The $\omega_s(x, y)$ profile shows a fourfold structure, while the amplitude of $\omega_d(x, y)$ shows a nearly elliptic structure. Change in the ϵ_v value produces maximum change in the magnitude of $\omega_s(x, y)$ and the qualitative structure of the d-wave order parameter component remains almost the same. These results are in agreement with the experimental observations of the fourfold symmetric structure of the order parameter component, indicating the presence of more than one order parameter component [2, 5, 16] in HTSs. Figure 3 shows the magnetic field distribution $B(x, y)$ for various values of the coupling parameter ϵ_v. Again, the lattice shows an oblique structure.

3.2. Local spatial behavior of the order parameters and the magnetic field

A major advantage of our numerical method over the earlier approximate studies is that it is possible to obtain the local spatial behaviors of the magnetic field and superconducting order parameter components such as the widths of the order parameters and the magnetic induction and their variation over the entire range of the applied magnetic field. The magnetic field dependence of the penetration depth is in general nonlinear. It has been suggested by Amin *et al* [38] that in the case of high T_c superconducting materials in states of mixed symmetry nonlinear and nonlocal effects are required to be considered, which affects the spatial distribution of the magnetic field component in the vortex lattice, specially at higher magnetic field inductions. Earlier calculations are only limited near upper or lower critical applied fields and the corresponding GL theories were treated in the linear limit; accordingly, it is not possible to see the nonlinear effects. We solve however the fully nonlinear GL equations. These local spatial behaviors are responsible for some of the experimentally observed properties of high T_c materials such as penetration depth, vortex core radius etc.

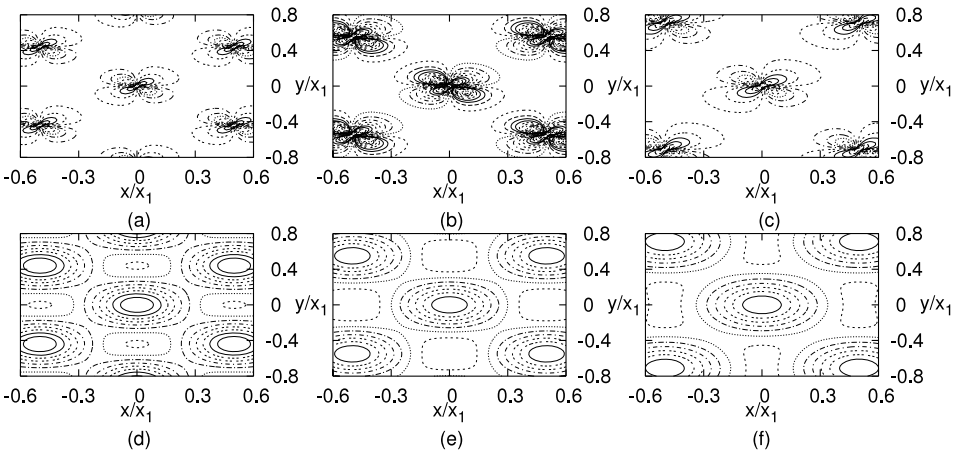

Figure 2. Contour plots of order parameter components. The parameter values are $\alpha_s/|\alpha_d| = 0.5$, $\beta_1/2\beta_2 = \beta_3/2\beta_2 = 1.0$, $\beta_4/2\beta_2 = 0.5$, $\phi = \pi/2$, $\kappa = 72$, magnetic induction parameter $b = 0.7$. (a)–(c) s-wave order parameter component $\omega_s(x, y)$ for $\epsilon_v = 0.1, 0.3$ and 0.4, respectively; (d)–(f) plots for the d-wave order parameter component $\omega_d(x, y)$ for $\epsilon_v = 0.1, 0.3, 0.4$, respectively.

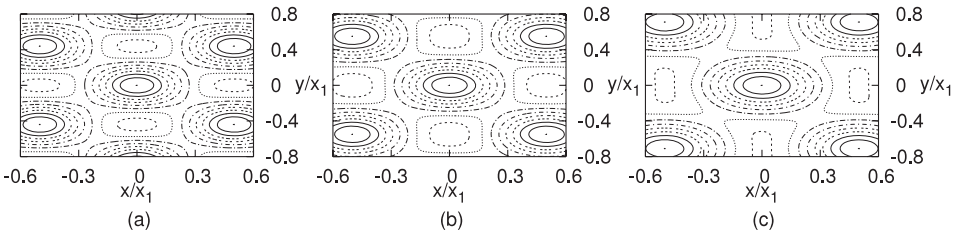

Figure 3. Contour plots for magnetic field component $B(x, y)$. Parameter values are the same as in figure 2.

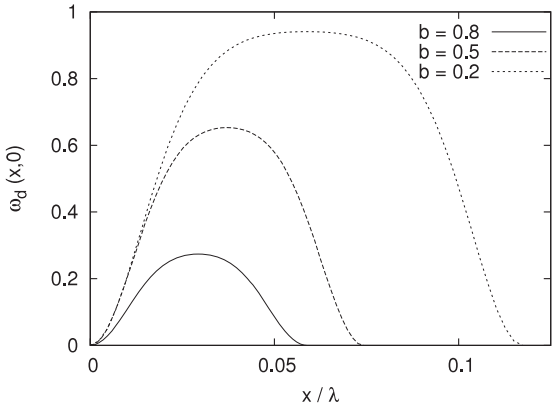

Figure 4. Spatial variation of the order parameter component $\omega_d(x, 0)$ along the x direction for different magnetic induction parameters b and coupling parameter $\epsilon_v = 0.1$. Other parameters are the same as in figure 2.

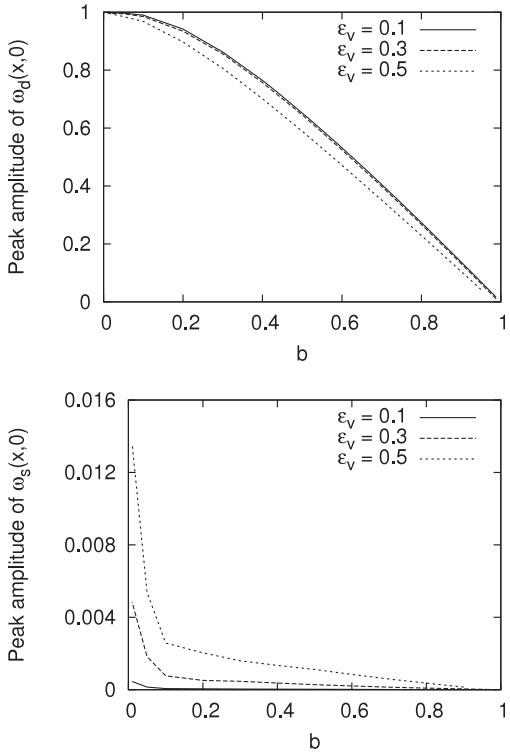

Figure 5. Variation of peak amplitude of the order parameter components $\omega_d(x, 0)$ and $\omega_s(x, 0)$ with magnetic induction b for different values of the coupling parameter ϵ_v. Other parameters are the same as in figure 2.

3.2.1. Order parameters. The spatial variation of the d-wave order parameter $\omega_d(x, 0)$ along a particular direction (x axis) for different values of the applied field is shown in figure 4. For $b \to 0, \omega \to 1$, which, as expected, is the isolated vortex limit. It can be seen from the figure that with increase of applied field the width of the order parameter (FWHM) decreases. This implies that the vortex core radius decreases with increasing field. This is in agreement with experiments on HTSs [39]. We discuss the vortex core radius further below. The s-wave order parameter also shows similar behavior. Figure 5 shows the variation of the peak amplitude of the order parameters $\omega_d(x, 0)$ and $\omega_s(x, 0)$ with applied field for various values of the coupling parameter ϵ_v. The s-wave component amplitude slightly increases with increase of the coupling parameter while that of the d-wave component decreases, but the overall amplitude of the s-wave component remains very small as compared to that of the d-wave component.

We now compare some of the results obtained from our analytical study of the two-order-parameter GL model with available experiments on HTSs. We first discuss the vortex core radius. It is well known that in a superconducting material the order parameter is strongly suppressed in the vicinity of the vortex core. This suppression of the superconducting electron density is not sharp and varies over a distance termed the coherence length, whose measure is comparable to the vortex core radius or size. Several attempts have been made to determine the vortex structure at arbitrary temperature, magnetic field and impurity concentration. Efforts were made to numerically solve the quasi-classical Eilenberger equations [40], which are a reformulation of the microscopic Gor'kov theory [41]. Kramer [42] determined the local structure of a vortex near H_{c1} by numerically solving the Usadel equations [43], and have found that with decreasing temperature the pair potential $\Delta(\mathbf{r})$, i.e the order parameter, rises more steeply and the magnetic field decays more rapidly as a function of distance from the center of the vortex.

We compare the magnetic field dependence of the vortex core radius $r_0(b)$ as obtained from our calculations with experimentally determined values of the vortex core size of HTSs $YBa_2Cu_3O_{6.95}$ [39]. For calculating the vortex core radius we have used the commonly used definition of vortex core size which comes from GL theory, where the core radius is defined as the FWHM of the calculated spatial dependence of the superconducting order parameter [44]. In figure 6, we have plotted the variation of the vortex core radius with the magnetic

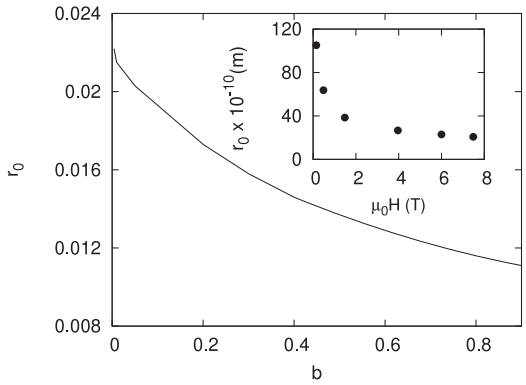

Figure 6. Variation of the vortex core radius with magnetic field. The inset shows the experimental data of the same for $YBa_2Cu_3O_{6.95}$ [39]. Parameter values used for the theoretical model are $\epsilon_v = 0.1$ and the other parameters are the same as in figure 2.

field as obtained from our two-order-parameter GL model. The vortex core radius decreases with increasing magnetic field. This is in agreement with the experimentally observed behavior (shown in the inset of the figure) of the variation of the vortex core radius with the applied field in $YBa_2Cu_3O_{6.95}$ [39]. We have also calculated the variation of the widths of the order parameter profiles with temperature in the mixed symmetry state of the HTSs. The widths so calculated give information about the coherence lengths of the system. To see the effects of the presence of two order parameter components and their couplings, we compute the temperature dependence of the widths of the order parameter profiles for different values of the coupling parameter ϵ_v. This is shown in figure 7.

It can be seen that the behavior remains qualitatively the same for different values of ϵ_v, but the magnitude of the widths increases with ϵ_v, indicating a broader vortex core at higher ϵ_v for all temperatures. Figure 8 shows the comparison of the variation of the vortex core radius with temperature as obtained from our analytic calculations with experimental data for the HTS $YBa_2Cu_3O_{6.95}$ [44]. The agreement between the analytical vortex core radius as computed from the two-order-parameter GL model and experimental results is very good. The vortex core radius decreases with decrease of temperature. We would like to mention here that the GL theory calculations become less accurate for temperatures far away from T_c as there are higher order terms which must be included in the GL free energy. Recently, Lipavský *et al* [45] proposed a method of extending the GL theory so as to make it applicable to all temperatures. It will be thus interesting to generalize this method for the two-order-parameter GL theory as considered here.

3.2.2. Magnetic field. We have studied the local spatial profile of the magnetic field induction for the two-order-parameter GL model of HTS. We have calculated the width of the magnetic field profile and studied the effect of the coupling parameter ϵ_v on the width. For a given value of ϵ_v, the width of the magnetic field profile depends on the magnetic induction parameter b. However, the shape of the curves remains qualitatively the same for different values of κ. The width of

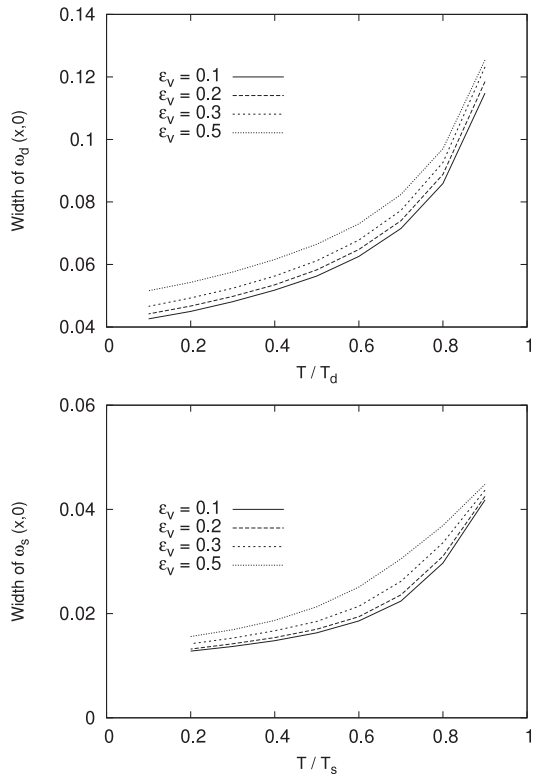

Figure 7. Widths of the order parameter profiles plotted against temperature for different values of the coupling parameter ϵ_v. The upper panel shows the variation of width of the d-wave order parameter component profile $\omega_d(x, 0)$ with temperature T/T_d. The lower panel shows the variation of the width of the s-wave order parameter component profile $\omega_s(x, 0)$ with temperature T/T_s. Parameter values are the same as in figure 2 and $b = 0.01$.

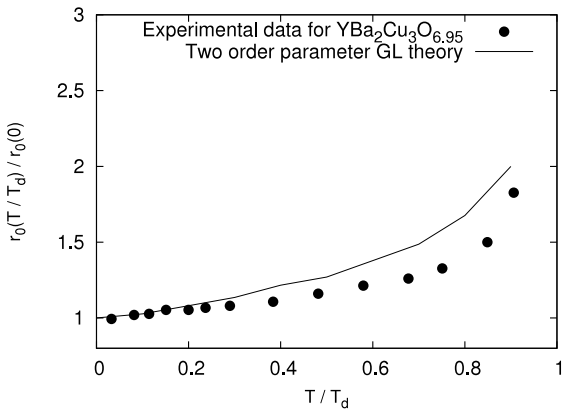

Figure 8. Temperature dependence of the vortex core radius. The solid line gives the theoretical result while the solid dots gives the experimental data for $YBa_2Cu_3O_{6.95}$ [44]. The parameter values used for the theoretical calculation are the same as in figure 2 with $b = 0.004$ and $\epsilon_v = 0.8$.

the profiles are plotted along a particular direction in the x–y plane, which we chose along the x axis. We define the width of the profile as the FWHM of the amplitude of the magnetic field profile. The widths so defined approximately give the characteristic length of the systems, i.e. the penetration depth. Figure 9 shows the variation of the width of the $B(x, 0)$ with

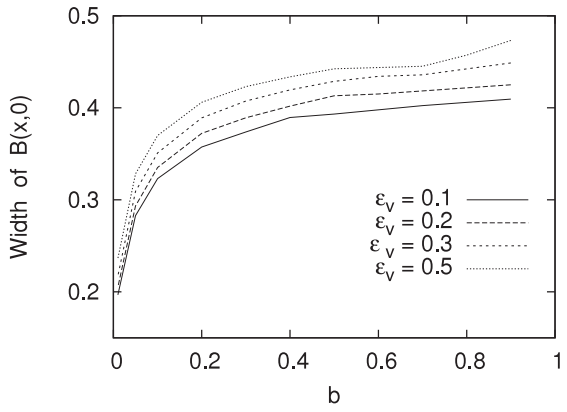

Figure 9. Variation of width of magnetic field profile $B(x, 0)$ with b for different values of coupling parameter ϵ_v. Other parameters are the same as in figure 2.

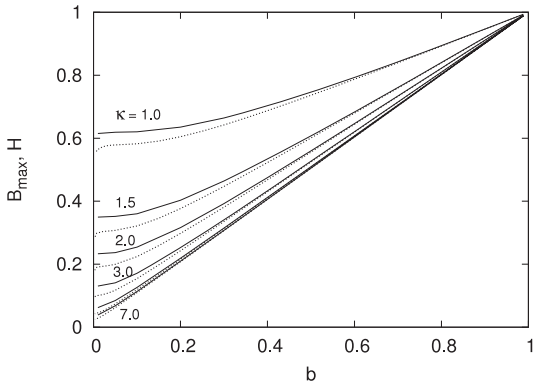

Figure 10. The maximum magnetic field B_{max} (upper solid lines) occurring at the vortex centers for the oblique vortex lattice compared with the applied magnetic field H (lower dashed lines) in the units of H_{c2}, plotted against magnetic induction $b = \bar{B}/B_{c2}$ for GL parameter $\kappa = 1.0, 1.5, 2.0, 3.0, 5.0, 7.0$. The other parameters used are the same as in figure 2, and $\epsilon_v = 0.1$.

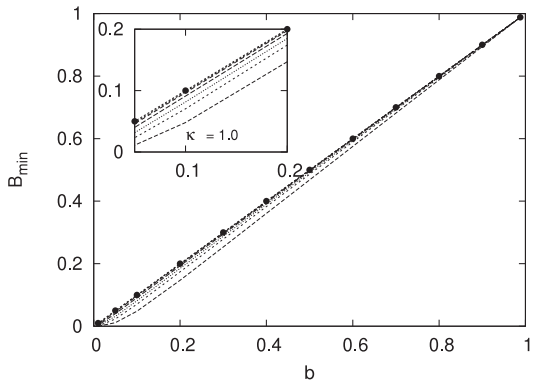

Figure 11. The minimum magnetic field B_{min} for the oblique vortex lattice is compared with the average magnetic induction $\bar{B}$ (dashed line with dots) in the units of H_{c2}, plotted versus b for GL parameter $\kappa = 1.0, 1.5, 2.0, 3.0, 5.0, 7.0$. Other parameters are the same as in figure 2 and $\epsilon_v = 0.1$.

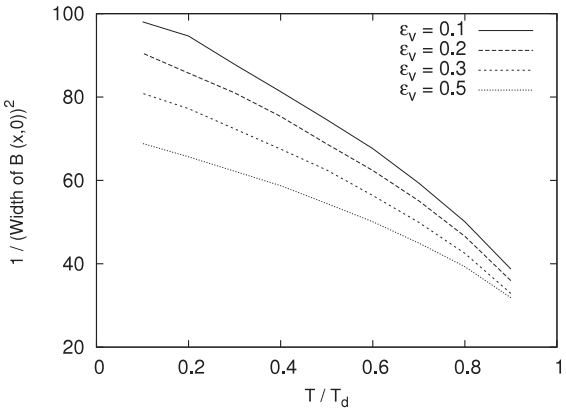

Figure 12. Variation of inverse square width of the magnetic field profile $B(x, 0)$ with temperature T/T_d for different values of the coupling parameter ϵ_v. Other parameters are the same as in figure 2 and $b = 0.01$.

coupling parameter ϵ_v. It can be seen that the width of the magnetic field profile increases with parameter ϵ_v.

We have also calculated the maximum B_{max}, the minimum B_{min} and the saddle point B_{sad} fields over the entire range of the applied magnetic field for various values of the GL parameter κ. These quantities are important for comparison with the muon spin rotation experiments of the high T_c materials [46]. Figure 10 shows the plot of the variation of B_{max} and applied magnetic field H with b. It can be see that the maximum magnetic field B_{max}, at the center of the vortex, always exceeds the applied magnetic field H. The minimum magnetic field B_{min} however lies below the average magnetic field $\bar{B}$, as shown in figure 11.

We now calculate the temperature dependence of penetration depth of the magnetic field and its variation with the coupling parameter ϵ_v. We also calculate the variation of the penetration depth with temperature and compare with experiment on HTSs. The penetration depth is defined as the distance over which the magnetic field profile varies in the superconductor. Experiments carried out on high T_c materials have suggested that the temperature dependence of the penetration depth is not linear and these observations have been attributed to the presence of nodes in the superconducting energy gap, which accounts for the sensitivity of the physical properties of these materials to impurities and crystalline defects. Amin *et al* [38] suggested that such a response of the magnetic penetration depth to temperature arises due to the influence of nonlinear and nonlocal effects on the vortex state of high T_c materials with mixed symmetry states. The influence of nonlocal effects is greater at higher magnetic field where the vortex density is greater and there is greater overlap of the regions in the vicinity of the vortex cores modified by the nonlocal effects. Thus, the linear T dependence of the penetration depth can be observed only at temperature above the energy scale of nonlinear and nonlocal effects. The variation of the inverse square of width of the magnetic field $B(x, 0)$ along the x-axis with temperature is as shown in figure 12. The width is defined as the FWHM of the field $B(x, 0)$, and it gives a measure of the penetration depth. It can be seen that the width increases with increase in temperature and the dependence is not linear. For a given temperature, the width increases with increase in the coupling parameter

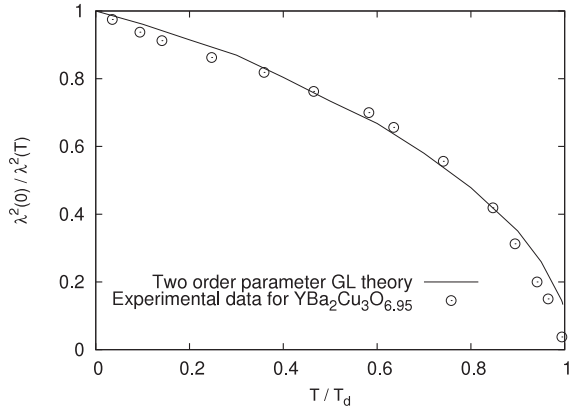

Figure 13. Variation of the ratio $\lambda^2(0)/\lambda^2(T)$ with temperature T/T_d. The solid line gives the theoretical result while the open circles gives the experimental data for $YBa_2Cu_3O_{6.95}$ [47]. The parameter values used for the theoretical calculations are the same as in figure 2; $b = 0.004$ and $\epsilon_v = 0.1$.

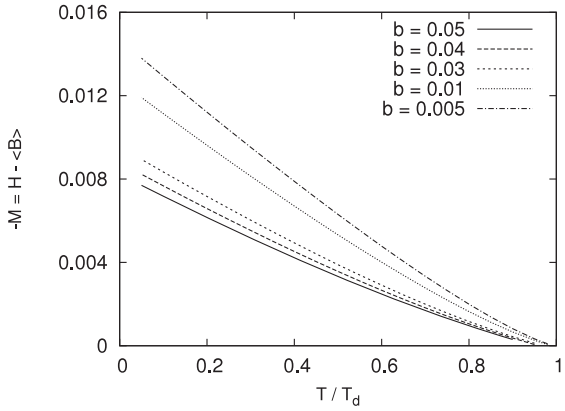

Figure 14. Variation of reversible magnetization (measured in the units of H_{c2}) with temperature for different values of the magnetic induction $b = 0.005, 0.01, 0.03, 0.04, 0.05$, respectively. Other parameter values are the same as in figure 2 and $\epsilon_v = 0.1$.

ϵ_v. To compare with experiment we calculate the variation of the penetration depth $\lambda(T)$ with temperature. Figure 13 shows the temperature (T/T_d) dependence of the ratio $(\lambda^2(0)/\lambda^2(T))$. The penetration depth $\lambda(T)$ as computed using our two-order-component GL theory is compared with the corresponding experimental data extracted from the $\Delta\lambda(T)$ measurement of $YBa_2Cu_3O_{6.95}$ crystal [47]. The agreement between the computed penetration depth using the two-order-parameter GL theory and the experiment is excellent.

3.3. Reversible magnetization

Yet another property of superconductors which can be computed numerically and compared with experiment is the reversible magnetization. Here we compute the variation of the reversible magnetization with the applied magnetic field and temperature and compare with experiments. Figure 14 gives the variation of reversible magnetization with temperature for different magnetic inductions. As expected, lower magnetic induction corresponds to lower magnitude of reversible magnetization. Figure 15 shows the comparison of the temperature dependence of reversible magnetization calculated using the two-order-parameter model with the experimental data for YBCO [48] for various applied field. The match between the analytical and the experimental results is again very good.

Reversible magnetization is an important quantity as it can be used to determine the upper critical magnetic field H_{c2} of HTSs. The upper critical field $H_{c2}(T)$ is a difficult quantity to determine due to large fluctuation effects in HTSs. The upper critical field $H_{c2}(T)$ obtained from the resistivity $(R(T))$ curves does not give an accurate result. Recently there have been arguments in the literature [18, 49, 50] about the origin of the observed unusual positive curvature in the variation of upper critical field H_{c2} with temperature. The positive curvature has been interpreted by some authors as evidence of the presence of multicomponent order parameters in the system [18, 49]. On the other hand, the unusual positive curvature of the $H_{c2}(T)$ curves derived from the

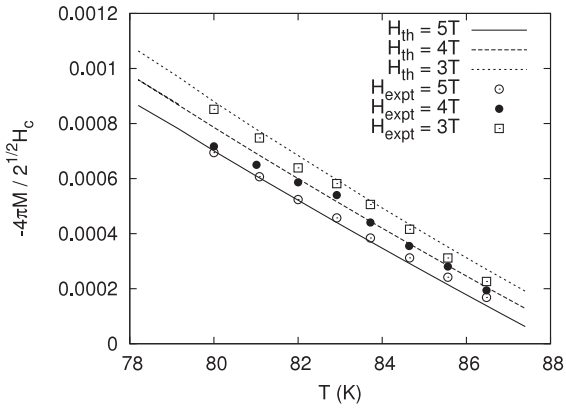

Figure 15. Comparison of theoretical temperature dependence of the reversible magnetization (denoted by H_{th}) with the experimental data for YBCO [48]. Parameters used for the theoretical calculations are $\kappa = 57$, $T/T_s = 0.5$, $\epsilon_v = 0.1$ and the other parameters are the same as in figure 2.

results of the resistance measurements is attributed to the misinterpretation of the resistance data [50]. It is therefore very important to know the correct behavior of the $H_{c2}(T)$ plots. H_{c2} obtained from the reversible magnetization gives a more accurate result. However, this approach has not been used so far, as earlier studies are limited to applied magnetic field near H_{c1} or H_{c2}. Since we can calculate the reversible magnetization for arbitrary applied magnetic field and as our method gives a numerically exact result, we are able to obtain H_{c2} very accurately from the computed reversible magnetization data. We have computed H_{c2} from the analytically obtained reversible magnetization by defining it as [50]

$$M(H, T) = (1/4\pi)(H_{c2}(T) - H)/(2\kappa^2 - 1)\beta_A. \quad (6)$$

Figure 16 shows the variation of the upper critical field H_{c2} with temperature for different values of the coupling parameter ϵ_v. It can be seen that the upper critical field $H_{c2}(T)$ increases slightly (as shown in the inset of the figure) with increase

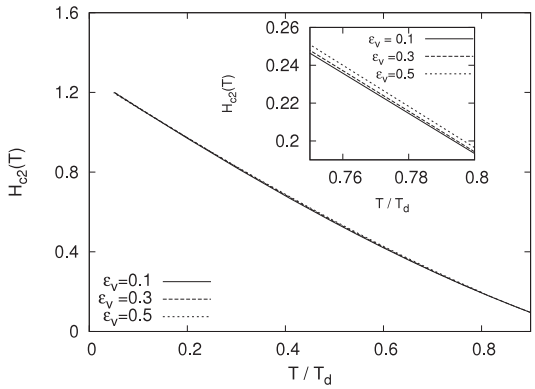

Figure 16. Variation of H_{c2} with temperature for different values of the coupling parameter ϵ_v at $T/T_s = 0.5$. Other parameters are the same as in figure 2 and $b = 0.01$.

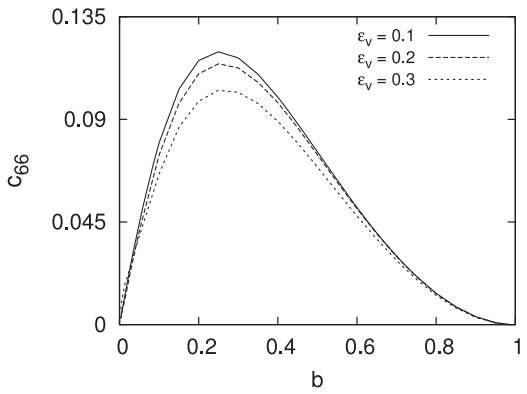

Figure 18. Variation of shear modulus of the vortex lattice with magnetic induction b for different values of coupling parameter ϵ_v. Other parameters are the same as in figure 2.

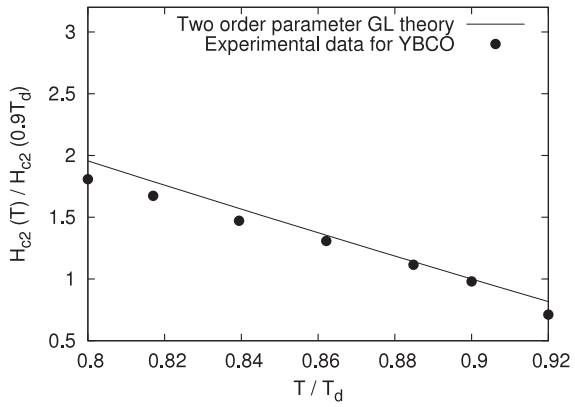

Figure 17. Comparison of the theoretical temperature dependence of the upper critical field $H_{c2}(T)$ (solid line) with the experimental data (solid dots) for YBCO [50]. Parameters used for the theoretical calculation are the same as in figure 2 with $b = 0.075$ and $\epsilon_v = 0.1$.

of the coupling parameter ϵ_v. This is in agreement with the earlier results that the increase of the coupling between the order parameters enhances the upper critical magnetic field $H_{c2}(T)$ [31]. The plot also shows a distinct upward curvature, which can be a signature of the presence of multicomponent behavior [18, 49]. Such behavior has been observed experimentally for both LSCO and YBCO [51, 52]. Figure 17 shows the comparison of the upper critical field $H_{c2}(T)$ calculated using our two-order-parameter GL model with the experimental data of YBCO [50]. The match between the theoretical and experimental results is fairly good.

3.4. Shear modulus (c_{66}) of the vortex lattice

Calculation of the shear modulus (c_{66}) is important for determining the stability properties of the vortex lattice such as the melting of the vortex lattice. Thermal fluctuations and softening of the vortex lattice may melt the vortex lattice and cause thermally activated depinning of the flux lines. Very recently, the Lindenmann criterion of vortex lattice melting has been formulated in terms of fluctuations of a single vortex over a characteristic length termed the single vortex length, and this length depends on the shear modulus (c_{66}) of the vortex lattice [53]. Experiments [54] have shown that the thermal fluctuations near critical temperature in high T_c materials leads to thermal depinning and entanglement of vortices, which in turn leads to softening of the vortex lattice and finally its melting.

We next compute the shear modulus of the vortex lattice of high T_c superconductors in the mixed symmetry scenario. For this, we determine the variation in the free energy density with lattice parameter x_2. We find that the free energy for constant unit cell height y_2 varies practically sinusoidally with x_2 for various values of the coupling parameter ϵ_v. The shear modulus (c_{66}) of this vortex lattice can thus be determined by the difference in the free energy density between a rectangular and an oblique flux line lattice and is given by the relation [46]

$$c_{66} = 2\pi^2[y_2(\epsilon_v)/x_1]^2 \times [f(x_2 = 0, y_2(\epsilon_v)) - f(x_2 = x_1/2, y_2(\epsilon_v))] \quad (7)$$

where $y_2(\epsilon_v)$ denotes the value of unit cell height which corresponds to the minimum free energy of the vortex lattice of a given symmetry for a given value of the coupling parameter ϵ_v. We have studied the behavior of the shear modulus with change of the coupling parameter ϵ_v and the results are shown in figure 18. The positive value of c_{66} suggests that the particular symmetry of the vortex lattice considered is stable. The plot looks qualitatively similar to that obtained for the single order parameter GL theory [46]. However, the peak position (b_{peak}) (the value of b for which c_{66} attains the peak value) and the peak amplitude of c_{66} changes for the two-order-parameter case considered here. The change in the value of ϵ_v affects both the peak amplitude and peak position of the shear modulus (c_{66}) of the vortex lattice. The peak position and the peak amplitude values of the shear modulus are important quantities. While the peak amplitude determines the hardness of the vortex lattice (stability of the vortex lattice), the peak position (b_{peak} value) denotes the magnetic induction at the peak value. Increasing the coupling parameter ϵ_v value results in a decrease in the peak amplitude of c_{66} as shown in figure 19. On the other hand, the value of the magnetic induction b_{peak} corresponding to this peak amplitude (peak position) increases with the increase in ϵ_v as shown in figure 20. The observations

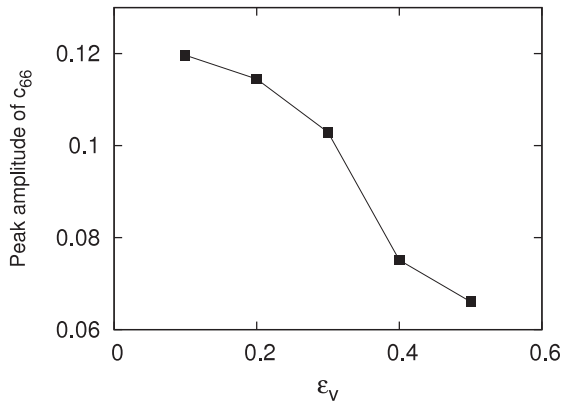

Figure 19. Variation of peak amplitude of c_{66} with different values of coupling parameter ϵ_v. Other parameters are the same as in figure 2.

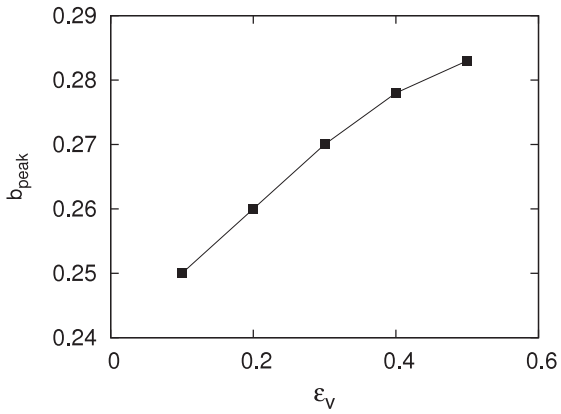

Figure 20. Variation of peak position of c_{66} with coupling parameter ϵ_v. Other parameters are the same as in figure 2.

are consistent with our observation of variation of magnetic penetration depth (λ), i.e. the width of the magnetic field profile $B(x, 0)$ with the coupling parameter ϵ_v. It is known that $1/\lambda^2 \approx c_{66}$, thus an increase in the penetration depth results in a decrease in the shear modulus (c_{66}) of the vortex lattice and vice versa. Since the increase in the coupling parameter value ϵ_v results in an increase in the penetration depth, it should decrease the shear modulus of the vortex lattice and thus the peak amplitude of c_{66}. Therefore, in the mixed symmetry states of the HTS the vortex lattice gets softened with increase of coupling parameter ϵ_v, and this favors its melting. The increase in the b_{peak} value with increasing coupling strength ϵ_v shows that for the HTS the vortex lattice will melt at higher magnetic field. This is in agreement with the vortex phase boundary as observed experimentally in single crystal of $YBa_2Cu_3O_{7-\delta}$ [54] and analytically in [53]. Figure 21 shows the plot of variation of the shear modulus with temperature for different magnetic field. It can be clearly seen that for a given value of b the shear modulus decreases with increasing temperature. Also it shows that for a given temperature the shear modulus decreases with increasing b. This implies that the melting of the vortex lattice is favored at higher temperature and also higher magnetic field. This agrees with the experimentally observed phase diagram of the vortex phase [54] and also the analytically obtained phase diagram for thermal melting of the vortex solid into the vortex liquid [53].

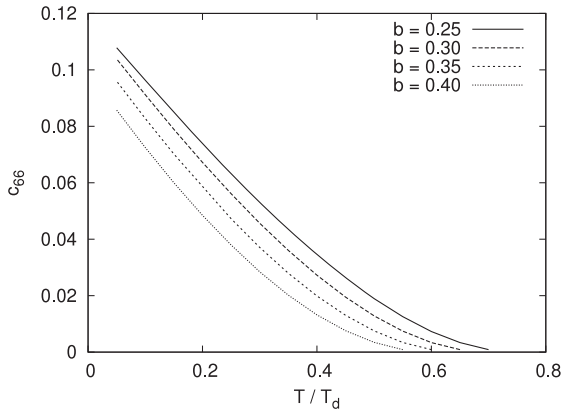

Figure 21. Variation of c_{66} with temperature for different values of magnetic induction b and coupling parameter $\epsilon_v = 0.1$. Other parameters are the same as in figure 2.

4. Conclusions

We have presented a detailed study of the properties of high temperature superconductors in states of mixed symmetry, focusing on the effects arising from s–d mixing. We have used a numerically exact method which is valid for the arbitrary applied magnetic field, GL parameter κ and vortex lattice symmetry. We have not used any ansatz for the form of the order parameters. We have obtained the structure of the single vortex and vortex lattices, width and amplitude of the order parameters and the induced magnetic field and their variations with the applied field and the coupling parameter ϵ_v representing the strength of the gradient coupling between the order parameters. We have for the first time calculated theoretically and compared with experiments several other properties of the HTSs in states of mixed symmetry, such as the temperature and applied magnetic field dependence of the vortex core radius, reversible magnetization and shear modulus of the vortex lattice and its relation to vortex lattice melting and also the variation of the penetration depth and upper critical magnetic field H_{c2} with temperature. From the fact that these properties are the signatures of the superconductivity phenomena and from the excellent agreement between the theoretical and experimental results, we make an important conclusion that the mixed symmetry scenario is a good candidate for the description of the high temperature superconductors.

However, we would like to mention that in the present work we have not considered the effects of anisotropy, thermodynamic fluctuation and hole concentration on the properties of HTSs. For a single order parameter GL theory we have recently shown how to take effects of anisotropy into account [55]. Similarly, Ginzburg [56] has suggested generalization of single-order-parameter GL theory by including a higher order term (ψ^6 term) in the GL free energy and making the coefficients of both the ψ^2 and ψ^4 terms temperature dependent, in order to take into account

the effect of thermodynamic fluctuations in high temperature superconductors. It is possible to extend these calculations for the two-order-parameter GL theory as considered here. However, similar calculations for the mixed symmetry scenario are very complex and are beyond the scope of the present paper. The effect of different hole concentrations can be taken into account by scaling the GL parameter κ by the inverse mean free path l. Such a scaled value of κ for a given hole concentration in $YBa_2Cu_3O_{7-\delta}$ is provided in [57].

Similar calculations may be useful to describe the properties of other multicomponent superconductors such as the heavy fermion superconductor UPt_3 [24]. The recently discovered superconducting material MgB_2 [58] has also revealed the presence of a multicomponent order parameter.

Acknowledgments

The authors would like to thank E H Brandt for help with the numerics. The authors would also like to thank University of Pune, Pune, India, for financial assistance through a BCUD research grant.

References

[1] Barret S E, Martindale J A, Durand D J, Pennington C H, Slichter C P, Friedmann T A, Rice J P and Ginsberg D M 1991 *Phys. Rev. Lett.* **66** 108
Martindale J A, Barrett S E, O'Hara K E, Slichter C P, Lee W C and Ginsberg D M 1993 *Phys. Rev.* B **47** 9155
[2] Wollman D A, Van Harlingen D J, Giapintzakis J and Ginsberg D M 1995 *Phys. Rev. Lett.* **74** 797
[3] Iguchi I and Wen Z 1994 *Phys. Rev.* B **49** 12388
[4] Tsuei C C, Kirtley J R, Chi C C, Lock See Y-J, Gupta A, Shaw T, Sun J Z and Ketchen M B 1994 *Phys. Rev. Lett.* **73** 593
[5] Mathai A, Gim Y, Black R, Amar A and Wellstood F C 1995 *Phys. Rev. Lett.* **74** 4523
[6] Devereaux T P, Einzel D, Stadlober B, Hackl R, Leach D H and Neumeier J J 1994 *Phys. Rev. Lett.* **72** 396
Devereaux T P and Einzel D 1995 *Phys. Rev.* B **51** 16336
[7] Hazen R M 1991 *Physical Properties of High Temperature Superconductors II* ed D M Ginsberg (Singapore: World Scientific)
[8] Li Q P, Koltenbah B E C and Joynt R 1993 *Phys. Rev.* B **48** 437
O'Donovon C and Carbotte J P 1995 *Phys. Rev.* B **52** 16208
Beal-Monod M T and Maki K 1996 *Physica* C **265** 309
[9] Heyen E T, Cardona M, Karpinski J, Kaldis E and Rusiecki S 1991 *Phys. Rev.* B **43** 12958
[10] Limonov M F, Rykov A I, Tajima S and Yamanaka A 1998 *Phys. Rev. Lett.* **80** 825
[11] Lu D H, Feng D L, Armitage N P, Shen K M, Damascelli A, Kim C, Ronning F, Shen Z X, Bonn D A, Liang R, Hardy W N, Rykov A I and Tajima S 2001 *Phys. Rev. Lett.* **86** 4370
[12] Miller J H Jr, Ying Q Y, Zou Z G, Fan N Q, Xu J H, Davis M F and Wolfe J C 1995 *Phys. Rev. Lett.* **74** 2347
[13] Ma J, Quitmann C, Kelley R J, Berger H, Margaritondo G and Onellion M 1995 *Science* **267** 862
[14] Sun A G, Gajewski D A, Maple M B and Dynes R C 1994 *Phys. Rev. Lett.* **72** 2267
Chaudhari P *et al* 1988 *Phys. Rev. Lett.* **60** 1653
[15] Aubin H, Behnia K, Ribault M, Gagnon R and Taillefer L 1997 *Phys. Rev. Lett.* **78** 2624
[16] Smilde H J H, Golubov A A, Arindo Rjinders G, Dekkers J M, Harkema S, Blank D H A, Roqalla H and Hilqenkamo H 2005 *Phys. Rev. Lett.* **95** 257001
[17] Annett J, Goldenfeld N and Legget A J 1996 *Physical Properties of High Temperature Superconductors* vol 5, ed D M Ginsberg (Singapore: World Scientific)
[18] Joynt R 1990 *Phys. Rev.* B **41** 4271
[19] Chakravarty S, Laughlin R B, Morr D K and Nayak C 2001 *Phys. Rev.* B **63** 094503
[20] Beal-Monod M T and Maki K 1996 *Europhys. Lett.* **33** 309
[21] Curras S R, Ferro G, Gonzalez M T, Ramallo M V, Ruibal M, Veira J A, Wagner P and Vidal F 2003 *Phys. Rev.* B **68** 094501
Ramallo M V, Pomar A and Vidal F 1996 *Phys. Rev.* B **54** 4341
[22] Keimer B, Shih W Y, Erwin R W, Lynn J W, Dogan F and Aksay I A 1994 *Phys. Rev. Lett.* **73** 3459
Maggio-Aprile I, Renner Ch, Erb A, Walker E and Fischer Ø 1995 *Phys. Rev. Lett.* **75** 2754
[23] Affleck I, Franz M and Amin M H S 1997 *Phys. Rev.* B **55** R704
[24] Joynt R 1997 *Phys. Rev. Lett.* **78** 3189
[25] Fisk Z, Hess D, Pethick C, Pines D, Smith J, Thompson J and Willis J 1988 *Science* **239** 33
[26] Volovik G E 1993 *Pis. Zh. Éksp. Teor. Fiz.* **58** 457
Volovik G E 1993 *JETP Lett.* **58** 469 (Engl. Transl.)
[27] Ren Y, Xu J and Ting C S 1995 *Phys. Rev. Lett.* **74** 3680
Xu J, Ren Y and Ting C S 1995 *Phys. Rev.* B **52** 7663
[28] Soininen P I, Kallin C and Berlinsky A J 1994 *Phys. Rev.* B **50** 13883
[29] Xu J, Ren Y and Ting C S 1996 *Phys. Rev.* B **53** R2991
[30] Heeb R, van Otterlo A, Sigrist M and Blatter G 1996 *Phys. Rev.* B **54** 9385
[31] Franz M, Kallin C, Soininen P I, Berlinsky A J and Fetter A L 1996 *Phys. Rev.* B **53** 5795
[32] Ichioka M, Enomoto N, Hayashi N and Machida K 1996 *Phys. Rev.* B **53** 2233
[33] Mel'nikov A S, Nefedov I M, Ryzhov D A, Shereshevskii I A and Vysheslavtsev P P 2000 *Phys. Rev.* B **62** 11820
[34] Li Q, Wang Z D and Wang Q 1999 *Phys. Rev.* B **59** 613
[35] Gohng J and Finnemore D K 1992 *Phys. Rev.* B **46** 398
[36] Abrikosov A 1957 *Sov. Phys.—JETP* **5** 1174
[37] Karmakar M and Dey B 2006 *Phys. Rev.* B **74** 172508
[38] Amin M H S, Affleck I and Franz M 1998 *Phys. Rev.* B **58** 5848
[39] Sonier J E, Brewer J H, Kiefl R F, Morris G D, Miller R I, Bonn D A, Chakhalian J, Heffner R H, Hardy W N and Liang R 1999 *Phys. Rev. Lett.* **83** 4156
[40] Eilenberger G 1968 *Z. Phys.* **214** 195
[41] Gor'kov L P 1958 *Sov. Phys.—JETP* **7** 505
Gor'kov L P 1959 *Sov. Phys.—JETP* **9** 1364
[42] Kramer L, Pesch W and Watts-Tobin R J 1974 *J. Low Temp. Phys.* **14** 29
[43] Usadel K D 1970 *Phys. Rev. Lett.* **25** 507
Usadel K D 1971 *Phys. Rev.* B **4** 99
[44] Sonier J E, Brewer J H and Kiefl R F 2000 *Rev. Mod. Phys.* **72** 769
[45] Lipavský P, Koláček J, Morawetz K and Brandt E H 2002 *Phys. Rev.* B **65** 144511
[46] Brandt E H 1997 *Phys. Rev. Lett.* **78** 2208
[47] Hardy W N, Bonn D A, Morgan D C, Liang R and Zhang K 1993 *Phys. Rev. Lett.* **70** 3999
[48] Hao Z, Clem John R, McElfresh M W, Civale L, Malozemoff A P and Holtzberg F 1991 *Phys. Rev.* B **43** 2844
[49] Kumar P and Wofle P 1987 *Phys. Rev. Lett.* **59** 1954
[50] Landau I L and Ott H R 2002 *Phys. Rev.* B **66** 144506
[51] Hidaka Y, Enomoto Y, Suzuki M, Oda M and Murakami T 1987 *Japan. J. Appl. Phys.* **26** L377
[52] Worthington T K, Gallagher W J and Dinger T R 1987 *Phys. Rev. Lett.* **59** 1160

[53] Kierfeld J and Vinokur V 2004 *Phys. Rev.* B **69** 024501
[54] Farrell D E, Rice J P and Ginsberg D M 1991 *Phys. Rev. Lett.* **67** 1165
[55] Achalere A and Dey B 2005 *Phys. Rev.* B **71** 224504
[56] Ginzburg V L 1988 *Physica* C **153–155** 1617
[57] Ossandon J G, Thompson J R, Christen D K, Sales B C, Kerchner H R, Thompson J O, Sun Y R, Lay K W and Tkaczyk J E 1992 *Phys. Rev.* B **45** 12534
[58] Nagamatsu J, Nakagawa N, Muranaka T, Zenitani Y and Akimatsu J 2001 *Nature* **410** 63